Chapter 7

Accuracy Analysis

7.1 Introduction

Relation (3.7) gives the 3-D coordinates of every point belonging to the laser curve. The purpose of this chapter, which is one of our original contributions, is to analyze the accuracy that one can expect on the position (x, y, and z) of a point P measured by mean of this formula.

For that, we consider three different types of errors that one can encounter, each of them being treated in a dedicated section:

- sampling errors (Section 7.2);
- speckle (Section 7.3);
- calibration (Section 7.4).

Concrete figures will be given in each case.

7.2 Sampling Errors

Sampling errors occur during image acquisition. They are due to the discrete character of a CCD sensor: an ICS coordinate will differ from its true value because the sampling process restricts image pixels to lie on an integer grid. At this point we suppose that the geometric parameters of the device have been exactly estimated through an appropriate calibration procedure. This question will be discussed in Section 7.4.

Sampling errors can be at most half a pixel in both x_{pix} and y_{pix} directions. Nevertheless, exploiting the fact that the laser curve generally has a width of several pixels and the mainly horizontal shape of the curve in the image, its center in the y_{pix} direction can be located with subpixel accuracy.

The whole procedure is detailed in Section 5.7.1, from which it appears that the sampling error Δy_{pix} in the y_{pix} direction is bounded to ± 0.15 pixel.

In the x_{pix} direction, the horizontal shape of the laser curve in the image does not permit subpixel accuracy. The corresponding error Δx_{pix} will thus be considered as ± 0.5 pixel.

Because their values are generally very small, angle ϵ of the laser plane (experienced value $\approx \pm 1°$) and skewness factor γ of the camera (experienced value $< \pm 10^{-3}$ pixel) are neglected in this chapter. We also suppose $f_x = f_y$, as it is generally the case in first approximation. Relation (3.7) thus becomes:

$$\begin{pmatrix} x \\ y \\ z \end{pmatrix} = \begin{pmatrix} \dfrac{x^*_{pix} y}{f_y} \\ \dfrac{e f_y}{y^*_{pix} + f_y \tan\delta} \\ \dfrac{y^*_{pix} y}{f_y} \end{pmatrix} \tag{7.1}$$

7.2.1 Accuracy on the y coordinate

The absolute error Δy on the y coordinate because of image sampling errors is expressed as the differential of y with regard to y_{pix} [using (7.1)]:

$$\Delta y = -\frac{e f \Delta y_{pix}}{(y_{pix} + f_y \tan\delta)^2} = -\frac{y^2 \Delta y_{pix}}{e f_y} \tag{7.2}$$

and is proportional to y^2 and Δy_{pix}, which was expected, seen that there is a loss of resolution at large y coordinates and that the worst the accuracy on the pixel location, the worst the estimation of y (at a proportional rate). Note that it does not depend on angle δ (for a given y), and that it is inversely proportional to the geometric parameters e and f_y.

From (7.2) we can easily express the relative error ρ_y on y:

$$\rho_y = \frac{\Delta y}{y} = -\frac{y \Delta y_{pix}}{e f_y} \tag{7.3}$$

Tables 7.1 and 7.2 present two typical situations that will be encountered in our applications (with D_a the lens aperture, that will be introduced in Section 7.3). A certain amount of tables in this section and in the next ones will refer to these two particular cases.

The first example (case 1) in Table 7.1 corresponds to the usual configuration of the instruments used in Chapters 9–11, and the second one (case 2) to that used in Chapter 12.

TABLE 7.1. Value of the geometric parameters for two particular situations

	f_y [pixel]	f [mm]	e [cm]	δ [°]	D_a [mm]
case 1	1280	8	10	3	10
case 2	30500	191	5	30	8

TABLE 7.2. x, y and z Ranges for two particular situations

	y range [cm]	z range [mm]	x range [mm]
case 1	$36 \ldots 400$	$-110 \ldots 81$	$-300 \ldots 300$
case 2	$9.82 \ldots 10.18$	$-8.8 \ldots -6.7$	$-1 \ldots 1$

TABLE 7.3 gives numerical values of Δy and ρ_y for the two particular cases of TABLES 7.1 and 7.2.

TABLE 7.3. Numerical Values of Δy and ρ_y for two Concrete Cases

	y range [cm]	Δy range [μm]	ρ_y range [%]	y [cm]	Δy [μm]	ρ_y [%]
case 1	$36 \ldots 400$	$152 \ldots 18750$	$0.04 \ldots 0.47$	100	1172	0.12
case 2	$9.82 \ldots 10.18$	$0.9 \ldots 1$	0.001	10	1	0.001

Unfortunately, in the second case, laser speckle will drastically affect the accuracy on y, so that the figure of 1 μm for Δy is not achievable in practice. This question will be discussed in Section 7.3.

7.2.2 Accuracy on the z coordinate

The absolute error Δz on the z coordinate because of image sampling errors is expressed as the differential of z with regard to y_{pix} [using (7.1)]:

$$\Delta z = \frac{e f_y \tan\delta \Delta y_{pix}}{(y_{pix} + f_y \tan\delta)^2} = -\Delta y \tan\delta \tag{7.4}$$

The same conclusions than with Δy thus apply, with one more observation: the smaller the angle δ, the better the accuracy on z (but also the more limited z range).

Since z is bound to y by (3.5) (where $\epsilon = 0$), it is thus possible to calculate z:

$$z = e - y \tan\delta \tag{7.5}$$

and the relative error ρ_z on z:

$$\rho_z = \frac{\Delta z}{z} = \frac{y^2 \Delta y_{pix} \tan\delta}{e f_y \left(e - y \tan\delta\right)} \tag{7.6}$$

TABLE 7.4 gives numerical values of Δz and ρ_z for the two particular cases of TABLES 7.1 and 7.2. Note that the same precautions than with Δy are to be taken regarding speckle in the second case.

TABLE 7.4. Numerical Values of Δz and ρ_z for two Concrete Cases

	z range [mm]	z [mm]	Δz [μm]	ρ_z [%]
case 1	$-110\ldots81$	48	61	0.13
case 2	$-8.8\ldots-6.7$	-7.7	0.6	0.007

7.2.3 Accuracy on the x coordinate

The accuracy on the x coordinate is a bit more complex to analyze since it will be influenced by both Δx_{pix} and Δy_{pix} and will vary with x and y. The absolute error Δx on this quantity because of image sampling errors is expressed as the differential on x with regard to Δx_{pix} and Δy_{pix} [using (7.1)]:

$$\Delta x = \left|\frac{e \Delta x_{pix}}{y_{pix} + f_y \tan\delta}\right| + \left|\frac{e x_{pix} \Delta y_{pix}}{\left(y_{pix} + f_y \tan\delta\right)^2}\right| = \frac{y}{e f_y}\left(\left|e \Delta x_{pix}\right| + \left|x \Delta y_{pix}\right|\right) \tag{7.7}$$

and is inversely proportional to e and f_y and independent from δ (for a given y), as it was the case with Δy.

From (7.7) we can easily express the relative error ρ_x on x:

$$\rho_x = \frac{\Delta x}{x} = \frac{y}{e f_y}\left(\left|\frac{e \Delta x_{pix}}{x}\right| + \left|\Delta y_{pix}\right|\right) \tag{7.8}$$

See TABLE 7.5 for some concrete figures concerning the two particular cases of TABLES 7.1 and 7.2.

TABLE 7.5. Numerical Values of Δx and ρ_x for two Concrete Cases

	x range [mm]	Δx [μm]	ρ_x [%]
case 1	$-300\ldots300$	742	0.25
case 2	$-1\ldots1$	1.6	0.16

Note that in the second case, because of the geometry of the system, $x\Delta y_{pix} << e\Delta x_{pix}$ in (7.7). Laser speckle—affecting Δy_{pix} only as it will be explained in Section 7.3—will thus not influence the accuracy on x, so that the figure of 1.6 μm for Δx is achievable in practice.

7.3 Speckle

As seen in the previous section, the accuracy on the WCS coordinates of a point P determined by (3.7) is directly affected by the accuracy at which the ICS coordinates of this point can be measured. It is also depending on the accuracy on the geometric parameters determined by calibration, as it will be discussed in the next section.

It would thus be tempting to believe that the only limit to the coordinate accuracy comes from image sampling errors and geometric considerations (i.e. bad estimation of the camera and laser plane parameters). However, there is also a physical limit, originating from speckle. A precise knowledge of it is of prime importance since it can prevent trying to push the technology toward unrealistic goals.

Speckle arises on the imaging sensor because, at each point of the image, the light wave amplitude is the result of the summation of contributions from all the scattering points of the object inside one pixel of the CCD sensor.

When the object is rough, on a scale comparable to the wavelength λ of the source—i.e. 630–670 nm in the case of a red laser—the summation involves phasors of random phases. For some portions of the image, these phasors cancel each other, leading to dark speckle, while for other parts of the image they tend to reinforce each other, creating bright speckle. See Fig. 7.1 for an image example of a laser stripe.

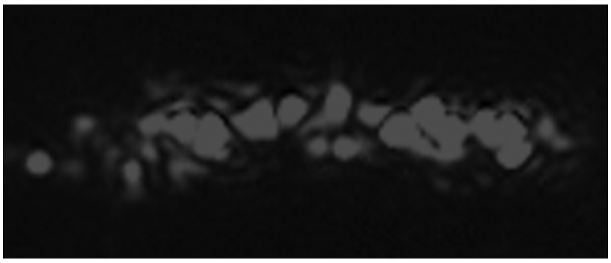

Fig. 7.1. Example of laser speckle. Close up on a laser stripe.

The influence of speckle on the accuracy of range finders using laser triangulation has been studied among others in [18] and [32].

Since it is a totally random process, the size and position of speckle grains is not predictable, and will change if the relative position between the imaging device and the target is modified. Nevertheless, a 3-D analysis of speckle patterns shows that they are cigar shaped and point away from the center of the lens. In a plane transversal to the camera plane, they are thus circular, and appears as circles on the CCD sensor as well. Their mean diameter D_s is expressed as [32]:

$$D_s = \frac{4\lambda f}{\pi D_a} \tag{7.9}$$

where D_a is the diameter of the lens aperture. TABLE 7.6 shows the mean speckle diameters D_s obtained in the two concrete cases of TABLE 7.1, where we considered $\lambda = 630$ nm (red laser) and the diaphragm of the lens opened at its maximum (i.e. 10 mm in case 1 and 8 mm in case 2, as in TABLE 7.1), which corresponds to the best situation.

TABLE 7.6. Numerical Values of D_s for two Concrete Cases

	D_s [μm]
case 1	0.6
case 2	19

The D_s figures of TABLE 7.6 have of course to be compared to the size of one pixel in the image to see if speckle will be of any influence in each of the concrete cases. The cameras we used in this work all had a square pixel size of 6.25 μm (see Section 4.2.1; this is indeed a standard value). We immediately see that the first example of TABLE 7.6 will not be influenced by speckle: the mean size of speckle grains is small enough. This will not be the case with the second example.

Without any particular precaution concerning reduction of the speckle effects, the consequences on the accuracy of y and z coordinates computed by (3.7) would be dramatic (imagine how difficult it would be to situate the center of a laser stripe looking like that of Fig. 7.1).

The accuracy on x is not affected by speckle. The process of structured lighting involves the detection of the laser curve center y_{pix} for each column of the image that the laser curve is occupying, i.e. for a series of x_{pix} values. The latter are "error-free", because fixed by the user. Nevertheless, x coordinate is also influenced by y_{pix}, which is affected by speckle, but as seen in Section 7.2.3, the error Δx introduced by a Δy_{pix} is negligible in comparison with that induced by a Δx_{pix}. To summarize: speckle only affects y_{pix}, which is of no influence on x, therefore speckle does not affect x.

Regarding y and z, we saw in Section 5.7.2 that it is actually possible to appropriately filter speckle, in order to limit its impact on the accuracy.

Simulations showed that an error Δy_{pix} of at most 1 pixel on the pixel location is achievable. TABLE 7.7 synthesizes all the figures of TABLES 7.3–7.5 taking speckle into account (the $\pm$ signs are omitted in front of each value, for sake of compactness).

TABLE 7.7. Numerical Values of the Absolute and Relative Errors on x, y and z for two Concrete Cases

	Δx_{pix} [pixel]	Δy_{pix} [pixel]	Δx [μm]	ρ_x [%]	Δy [μm]	ρ_y [%]	Δz [μm]	ρ_z [%]
case 1	0.5	0.15	712	0.25	1200	0.1	61	0.13
case 2	0.5	1	1.7	0.17	6.6	0.007	3.8	0.05

7.4 Calibration Errors

In this section we focus on the accuracy that one can expect on the position (x, y, and z) of a point P if the values of the camera and laser plane parameters are inaccurate (e.g. because of a bad calibration or shocks on the instrument inducing a shift of the parameter values).

We will refer the results in this section to the two particular situations exposed in TABLES 7.1 and 7.2, and regarding the errors on the parameters, we will assume that they equal to the experimental standard deviations found in Chapter 6: $\rho_e = \rho_\delta = 0.06\%$ and $\rho_f = 0.12\%$.

7.4.1 Error due to a bad estimation of e

The relative error $\rho_{y,e}$ on the y coordinate because of a bad estimation of distance e is expressed as the differential of y with regard to e, divided by y [using (7.1)]. The same goes for the x and z coordinates, yielding:

$$\rho_{x,e} = \rho_{y,e} = \rho_{z,e} = \rho_e \tag{7.10}$$

The error on e is thus directly transferred on the coordinates. See TABLE 7.8 for concrete figures.

7.4.2 Error due to a bad estimation of f

Using the same principle than with e, we find:

$$\begin{aligned} \rho_{y,f} &= \rho_f \left(1 - \tfrac{y \tan \delta}{e}\right) \\ \rho_{x,f} &= \rho_{z,f} = -\rho_f \tfrac{y \tan \delta}{e} \end{aligned} \tag{7.11}$$

TABLE 7.8. Numerical Values of the Absolute and Relative Errors Due to a Bad Estimation of e

	ρ_e [%]	Δx_e [μm]	$\rho_{x,e}$ [%]	Δy_e [μm]	$\rho_{y,e}$ [%]	Δz_e [μm]	$\rho_{z,e}$ [%]
case 1	0.06	18	0.06	600	0.06	29	0.06
case 2	0.06	0.6	0.06	60	0.06	4.6	0.06

As we see, the relative errors depend on the laser plane parameters, but also on y. TABLE 7.9 gives numerical values of the relative errors for the two particular cases of TABLES 7.1 and 7.2. We see that in case 1, the error on the coordinates is attenuated by a factor 2; in case 2, y coordinates is almost not influenced by an error on f, contrarily to x and z.

TABLE 7.9. Numerical Values of the Absolute and Relative Errors Due to a Bad Estimation of f

	ρ_f [%]	Δx_f [μm]	$\rho_{x,f}$ [%]	Δy_f [μm]	$\rho_{y,f}$ [%]	Δz_f [μm]	$\rho_{z,f}$ [%]
case 1	0.12	189	(−) 0.06	571	0.06	30	(−) 0.06
case 2	0.12	1.4	(−) 0.14	18.5	(−) 0.02	10.7	(−) 0.14

7.4.3 Error due to a bad estimation of δ

For sake of easiness, we will consider the relative error on $(\tan\delta)$ instead of δ to study the relative errors on x, y and z. Using the same principle than with e and f, we find:

$$\rho_{x,\delta} = \rho_{y,\delta} = \rho_{z,\delta} = -\rho_\delta \frac{y\tan\delta}{e} \tag{7.12}$$

Again, the relative errors depends on the laser plane parameters and on y. TABLE 7.10 gives numerical values of the relative errors for the two particular cases of TABLES 7.1 and 7.2. In case 1, the error on the coordinates is attenuated by a factor 2; in case 2, it is slightly amplified.

7.5 Summary

The data of TABLES 7.7–7.10 are summarized in TABLE 7.11, where we made the pessimistic supposition that the final error on a coordinate (x, y or z) is the sum of all the error terms coming from the different sources of errors.

TABLE 7.10. Numerical Values of the Absolute and Relative Errors Due to a Bad Estimation of $\tan\delta$

	ρ_δ [%]	Δx_δ [μm]	$\rho_{x,\delta}$ [%]	Δy_δ [μm]	$\rho_{y,\delta}$ [%]	Δz_δ [μm]	$\rho_{z,\delta}$ [%]
case 1	0.06	94	(−) 0.03	314	(−) 0.03	15	(−) 0.03
case 2	0.06	0.7	(−) 0.07	69	(−) 0.07	5.4	(−) 0.07

TABLE 7.11. Numerical Values of the Absolute and Relative Errors Due to Image Sampling, Speckle and Calibration

	Δx [μm]	ρ_x [%]	Δy [μm]	ρ_y [%]	Δz [μm]	ρ_z [%]
case 1	1205	0.4	2657	0.27	135	0.28
case 2	4.4	0.44	154	0.15	24.5	0.32

At this point, the only observation that we can make is that the error on the coordinates is of a few tenths of a percent. This will be taken into account when we evaluate the expected accuracy of the devices developed in Part II.

Note that these figures suppose that the mechanical parts of the instruments are sufficiently robust, in order to prevent the parameter values from changing when the instrument is manipulated (which would invalidate the whole calibration procedure).